Lab on a Chip

PAPER

View Article Online
View Journal | View Issue

Cite this: *Lab Chip*, 2019, **19**, 1633

A high-speed, high-performance, microfabricated comprehensive two-dimensional gas chromatograph

Joshua J. Whiting,*[a] Edward Myers,†[b] Ronald P. Manginell,[a] Mathew W. Moorman,[a] John Anderson,[ac] Cory S. Fix,‡[a] Cody Washburn,[d] Al Staton,§[a] Daniel Porter, ¶[a] Darin Graf,||[a] David R. Wheeler,[e] Stephen Howell,**[d] John Richards,[f] Haley Monteith,[a] Komandoor E. Achyuthan, [a] Michael Roukes[b] and Robert J. Simonson††[a]

Received 9th January 2019,
Accepted 18th March 2019

DOI: 10.1039/c9lc00027e

rsc.li/loc

A small, consumable-free, low-power, ultra-high-speed comprehensive GC×GC system consisting of microfabricated columns, nanoelectromechanical system (NEMS) cantilever resonators for detection, and a valve-based stop-flow modulator is demonstrated. The separation of a highly polar 29-component mixture covering a boiling point range of 46 to 253 °C on a pair of microfabricated columns using a Staiger valve manifold in less than 7 seconds, and just over 4 seconds after the ensemble holdup time is demonstrated with a downstream FID. The analysis time of the second dimension was 160 ms, and peak widths in the second dimension range from 10–60 ms. A peak capacity of just over 300 was calculated for a separation of just over 6 s. Data from a continuous operation testing over 40 days and 20 000 runs of the GC×GC columns with the NEMS resonators using a 4-component test set is presented. The GC×GC-NEMS resonator system generated second-dimension peak widths as narrow as 8 ms with no discernable peak distortion due to under-sampling from the detector.

Introduction

Since the introduction of the first microfabricated gas chromatograph (μGC) by Terry *et al.* in 1979,[1] continuing effort has gone into improving the chromatographic performance of microfabricated columns through column design, coating, and modeling. Extensive reviews of the current state of the field have recently been published by Ghosh *et al.*[2] and Regmi and Agah,[3] that chronicle many of the challenges and best practices. With the use of existing models to aid in intelligent design, columns may be routinely fabricated to generate 4000–6000 theoretical plates per meter for separations of test alkane mixtures.[4–6] However, many of these columns are unsuitable for very high-speed applications because their separation performance degrades severely as the linear carrier gas velocity approaches and exceeds 100 cm s^{-1}, significantly exceeding the Golay minimum.[6–8] For time-sensitive applications such as the detection of chemical weapons, this loss of separation performance results in a compromise between false alarm rate and detection speed. Improved high-speed GC performance is necessary to meet this need.

Researchers at the University of Michigan, Sandia National Laboratories, and Louisiana State University demonstrated that column geometry can have a significant impact on the high-speed performance of microfabricated columns.[9] Likewise, theoretical predictions of height equivalent to a theoretical plate (HETP) for rectangular columns as developed by Golay, Spangler and Ahn over the past 40 years have added to our understanding of how to improve the performance of microfabricated columns.[10–13] Incorporating these insights, a significantly improved high speed performance polar microfabricated column has been demonstrated by Sandia

[a] *Nano and Micro Sensors, Sandia National Laboratories, Albuquerque, NM 87185, USA. E-mail: jjwhiti@sandia.gov*
[b] *Kavli Nanoscience Institute, California Institute of Technology, Pasadena, CA91125, USA*
[c] *III-V Microelectronics, Sandia National Laboratories, Albuquerque, NM 87185, USA*
[d] *Applied Technologies, Sandia National Laboratories, Albuquerque, NM 87185, USA*
[e] *Special Technologies, Sandia National Laboratories, Albuquerque, NM 87185, USA*
[f] *Autonomy for Hypersonics, Sandia National Laboratories, Albuquerque, NM 87185, USA*
† No longer at Caltech, current email address is ed.ben.myers@gmail.com
‡ No longer at Sandia, current email address is csfix1@gmail.com
§ Retired from Sandia National Laboratories.
¶ No longer at Sandia, current email address is xquicksilverx@gmail.com
|| No longer at Sandia, current email address is darin@gentechconcepts.com
** Ex-Sandia National Laboratories staff member.
†† No longer at Sandia, current email address is jandksimonson@msn.com

National Laboratories.[14] With these advances, high speed performance is significantly improved; however, the chemical information provided by these systems (retention time and peak area) is still insufficient in a one-dimensional chromatographic separation to adequately reduce the incidence of false positive chemical identifications caused by potential interferants or coelutions in some applications. Over the past decade researchers have sought to increase the resolving power of these microfabricated columns by integrating these devices into comprehensive multidimensional GC systems (GC×GC). This includes work at the University of Michigan (Zellers, Wise, and Kurabayashi groups) on a microfabricated thermal modulator,[15–18] and preliminary work presented at Transducers 2009, by Sandia on the developments reported here.[19]

Significant effort over the years has gone into the development of modulator designs to improve performance, reliability, and capability of comprehensive two-dimensional gas chromatography (GC×GC). The late John Phillips[20] is credited with developing the first modulator which consisted of a thick-phase capillary column wrapped with wires and had the outside coated with electrically conductive paint. Electrical pulses were used to resistively heat the modulator and liberate any trapped components in the thick phase. These modulators were tedious to build and sometimes suffered failure due to overheating, so the next evolution of modulator was the more robust rotating slotted heater. The heater was aligned so that the slot matched the capillary axis and thus the capillary would be periodically heated from two sides as the rotating heater passed by.[21] Another major modulator design was Mariott's longitudinally-modulated cryogenic system (LMCS) which used a mobile cryotrap that surrounded a section of the capillary and moved back and forth in order to create two stages of trapping.[22] One more thermal modulator design is the cold and hot jet design which uses the jets aimed at the column to cool it during analyte trapping and heat it during analyte release. This modulator has become popular due to its robustness, trapping efficiency, and lack of moving parts.[23] Thermal modulator technology is now commercially available from several vendors including LECO, Agilent, and Zoex Corporation.

The earliest reports of valve modulation date back to the Synovec lab at the University of Washington in 1998,[24] while this initial system was not entirely comprehensive – as it utilized a split flow to enable very sharp injection plugs onto the secondary column – it offered a path to much faster GC×GC separations without the need for cryogens than had been traditionally done to that point. 6-port valve-based modulators also suffer from potential analyte loss and/or contamination from passing thru the valve itself. While many valve bodies and sealing materials are chosen to minimize this; for particularly "sticky" compounds such as low-vapor pressure, highly-polar species, like many CWAs and their surrogates, this can be a concern. In 2001, the Seeley lab at Oakland University first published on their differential flow modulator.[25] The differential flow modulator solved this problem by placing the valve outside of the flow path of the sample and outside the oven, it also thereby enabled higher run temperatures extending the range of compounds that could be analyzed by the technique, and leading to the first commercially available consumable-free modulator.[26] The design uses a pair of secondary columns and the effluent from the primary column was switched between them at a known modulation frequency. Pulsed flow modulation (PFM) developed by the Shellie lab at the University of Tasmania eliminates the need for a second secondary column simplifying analysis and enabling a truly comprehensive GC×GC analysis.[27] Recently, the Seely lab refined the PFM modulator further to enable a single modulator setup to operate in multiple multidimensional modes – heart cut and both low and high duty cycle GC×GC.

The Sacks lab at the University of Michigan developed portable GC×GC systems for aerospace and environmental applications for several years, with a significant emphasis on eliminating the need for a cryogen for cooling the thermal modulator. That work focused on two paths: first, replacing the cryogen with chilled air,[28,29] and second, utilizing micromachined modulator designs having reduced thermal masses.[30] Both of these methods are promising; however, for chemical analysis applications where available power is limited, such as handheld or portable environmental monitoring instrumentation, the rapid heating and cooling of even a micromachined thermal modulator requires a prohibitive amount of power. For successful application of GC×GC methods under such conditions an alternate method must be explored.

The GC×GC modulator may in general be considered as having a two-state duty cycle. The purpose of the modulator during one state of this cycle is to stop a given elution band's migration at the end of the first column, long enough for an entire second column separation to occur. In the second state of the duty cycle, the modulator must then promote band migration at the end of the first column, resulting in injection of the next sample aliquot onto the second column. The band migration velocity of the chemical component i at the modulator, u_{im}, is given by eqn (1), where u_m is the linear carrier gas velocity at the modulator, and k_{im} is the retention

$$u_{im} = \frac{u_m}{(k_{im} + 1)} \quad (1)$$

factor of component i at the modulator. It is clear from this equation that the band migration velocity of component i can be driven toward zero by either increasing the retention factor toward infinity or by decreasing the linear carrier gas velocity to zero. Traditional thermal modulators act by modulating k_{im}; however, for very volatile species, including permanent gases, k typically cannot be increased sufficiently to trap the analyte on the modulator. Conversely, for chemical components of very low volatility, k can often not be decreased enough to get sharp injections onto the second column. Both

of these volatility extremes result in losses of resolving power. By modulating the carrier gas velocity, u_m, instead of the retention factor, the modulation efficiency is independent of the component volatility, thus allowing a wider range of analytes to be modulated.

Sacks, *et al.*[31–36] at the University of Michigan demonstrated the utility of modulating the flow at the junction point of series coupled columns of differing selectivity, to enhance the separation of a known mixture. In that work, the junction point of the two columns was connected to an electronic pressure controller, thus allowing the pressure at that junction point to be varied independently of the system inlet pressure, *i.e.*, the carrier gas pressure maintained at the inlet of the first column. By modifying the junction pressure throughout a separation, the effective contributions of the two columns to the overall retention factor of the column ensemble could be modified, enhancing the overall separation and minimizing the overall analysis time by utilizing the available peak capacity more efficiently. Those efforts culminated in the development of the stop-flow modulation system.[37–39] In this special case the junction point pressure could be temporarily set equal to the inlet pressure, effectively stopping the flow on the first column and increasing the flow on the second column. If, during a separation at constant inlet pressure and constant junction pressure, two peaks were found to be separated by the first column but then recombined and coeluted from the second column, then during subsequent analyses a valve connecting the junction point to a pressure source equal to the inlet pressure could be opened after the first component eluted from the first column onto the second column, but before the second component eluted onto the second column. During the resulting stop flow event the analyte on the first column stops its migration, and the analyte on the second column increases its migration. When the valve is closed again the flow resumes its normal profile and the analytes are separated by a length of time roughly equal to the duration of the stop-flow pulse.

The stop-flow technique has also been used to modulate the flow for a thermal/pneumatic modulator as described by Harynuk and Gorecki at the University of Waterloo.[40] In that work, a six port valve was used in conjunction with a thermal modulator to decouple the modulation period and the analysis time on the second column. The primary column was connected to the valve, along with a bypass column which was connected to both the inlet pressure source and to the secondary column through a thermal modulator. In that arrangement, when the valve is in the loading position carrier gas flows through the primary column and carries sample onto the thermal modulator. When the valve switches, flow goes through the bypass column instead. The dimensions of the bypass column were chosen to match the flow impedance of the primary column, so that flow into the thermal modulator was constant. The thermal modulator was then rapidly heated, injecting the focused sample onto the secondary column. During this injection period the flow on the primary column is stopped, and flow on the bypass-second column combination is maintained near the optimal velocity. This allows the analysis on the secondary column to progress at a velocity closer to the optimum thus increasing the secondary column resolving power. This process is repeated at a known frequency resulting in a modulated signal.

In the present work a modification of this technique is described, which eliminates the thermal modulator. The carrier gas pressure source is instead connected through a single 2-way valve with a tee joining the primary and secondary columns, as illustrated schematically in Fig. 1A. While this configuration is similar to that used by Whiting and Sacks,[38] in this work the pressure at the junction point between the columns is periodically modulated by opening and closing the 2-way valve. Under these conditions, when the valve is closed a small amount of material elutes from the first column onto the second column. The flow rate at the junction point during this elution is relatively slow, because the total flow impedance between the inlet pressure source and the system outlet is the sum of the impedances of the first and second GC columns. When the valve opens, this material is separated on the second column. The flow rate on the second column during this condition is increased, due to the decrease in total gas flow impedance achieved by bypassing the first GC column. This method enables a comprehensive GC×GC modulation at relatively fast modulation periods (<1 s) without the use of a cryogen. Because the modulation period can be adjusted from tens of milliseconds to tens of seconds, even narrow elution bands can be "sliced" or subdivided into multiple injections onto the second column. Therefore, high-speed gas chromatography techniques (microbore columns, high speed temperature programming, hydrogen as carrier gas, *etc.*) can be utilized in conjunction with the technique to minimize analysis time.

The drawback of this method, relative to more established thermal GC×GC modulation, is the loss of elution band focusing achieved at the junction point. Such focusing can sharpen peaks and enhance detectability of lower concentration analytes. This method offsets some of this loss in detectability enhancement because the differential flow between loading of the second column and detection. This results in a gas compression roughly equal to the ratio of two flows yielding a nearly comparable detectability enhancement.

Experimental section

Apparatus

Fig. 1A shows a schematic of the test system where CG is the carrier gas, I is the inlet, C1 is a non-polar polydimethyl siloxane (PDMS) coated column and C2 is a polar polyethylene glycol (PEG) coated column, D is the detector, and V is a valve used to modulate the pressure at the junction point to enable stop-flow modulation. The columns were connected at the junction point by a Siltek-treated, low dead-volume "*Y*" (Restek, Corp. Bellefonte, PA), with the third leg of the "*Y*" connected to the valve modulator manifold through a short length (~5–10 cm) of 530 μm inner diameter deactivated

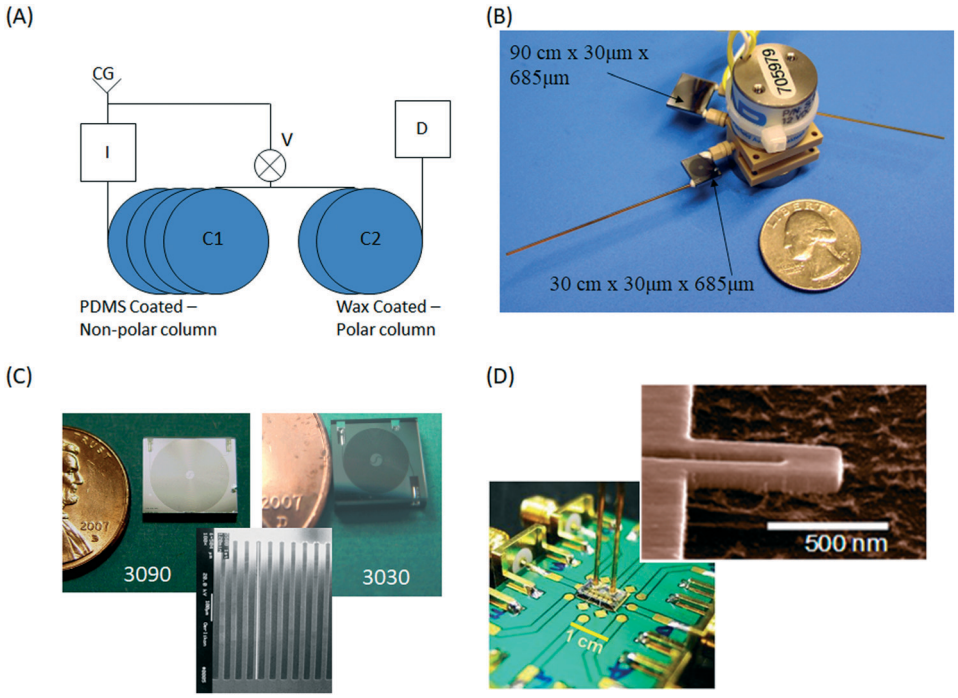

Fig. 1 (A) Schematic of the test system where CG is the carrier gas, I is the inlet, C1 is a non-polar polydimethyl siloxane (PDMS) coated column and C2 is a polar polyethylene glycol (PEG) coated column, the D is the detector, and V is a valve used to modulate the pressure at the junction point to enable stop-flow modulation. (B) Neptune research valve manifold with 3090 and 3030 microfabricated columns. (C) 3090 and 3030 microfabricated columns each with a cross section of nominally 30 μm wide × 685 μm deep. The 3090 is 90 cm long and coated with a non-polar PDMS stationary phase. The 3030 is 30 cm long and coated with a polar PEG stationary phase. (D) Caltech NEMS resonator detector, packaged and unpackaged.

fused silica tubing (Restek, Corp.). The columns were connected to the split/splitless inlet and the flame ionization detector (FID) of an Agilent 6890 controlled by ChemStation software (Agilent Technologies, Santa Clara, CA) for most experiments. The inlet was operated in constant pressure mode with the split mode with the split ratio set to the maximum allowed by software for each experiment to minimize injection plug width. The electrometer of the FID was replaced with DHPCA-100 high speed variable gain current amplifier from FEMTO (Berlin, Germany). The signal from the DHPCA-100 was recorded *via* a NI-6008 USB DAQ using custom software developed in LabView 7.2 (National Instruments, Austin, TX), which also controlled valve timing, GC heater timing, and recorded column temperatures. Samples were injected using an Agilent 7683 series autosampler and injector equipped with a 10 μL syringe. The utilization of the constant pressure inlet control resulted in flow rates varying throughout the analysis as the stop-flow valve was opened and closed, the flow ratio was roughly 5 : 1 for all experiments. Flow thru the MEMS columns switched from ~0.5 mL min^{-1} to ~2.5 mL min^{-1} hydrogen for the work presented here.

The valve modulator manifold went through three design revisions as part of this work, the initial work with commercial capillary columns shown in Fig. 2A – which consisted of a 1 m length of 100 μm diameter fused silica coated with a 0.1 μm film of PDMS (RTX-1, Restek) and 1 m length of 100 μm diameter fused silica coated with a 0.1 μm film of PEG (RTX-WAX, Restek) – was performed using pneumatically-actuated valve (MOVP, SGE, Austin, TX). The initial work with microfabricated columns utilized a custom valve and valve manifold from Neptune Research (West Caldwell, NJ) shown in Fig. 1B and used to collect the methane data shown in Fig. 2B. This valve was replaced by the Staiger Spider valve (Erligheim, Germany) which was used to collect the remaining data.

Fig. 1C shows the two microfabricated column designs used for the work presented here. The cross section of both columns was nominally 30 μm wide × 685 μm deep as shown, but with differing lengths and coatings. The first 30 μm wide column was 90 cm in length, and was designated "3090", and coated with polydimethyl siloxane. The second column was 30 cm in length, was given a designation of "3030", and coated with polyethylene glycol. Both columns were laid out in a "spiral-in-spiral-out" geometry with edge connections. The fluidic connections to both columns were provided by a short length (<3 cm) of thick walled fused silica capillary tubing with a nominal internal diameter of 150 μm and a nominal outer diameter of 665 μm (Polymicro Technologies, Phoenix, AZ P/N-150665). The capillary columns were passivated with Silyl-8 (Pierce Biotechnology, Inc., Rockford, IL) prior to assembly. These capillary interconnects were secured into 720 μm wide × 685 μm deep ports on the edges of the columns using a two-part high temperature epoxy Hysol 1C (Henkel, Dusseldorf, Germany). This thick-walled tubing

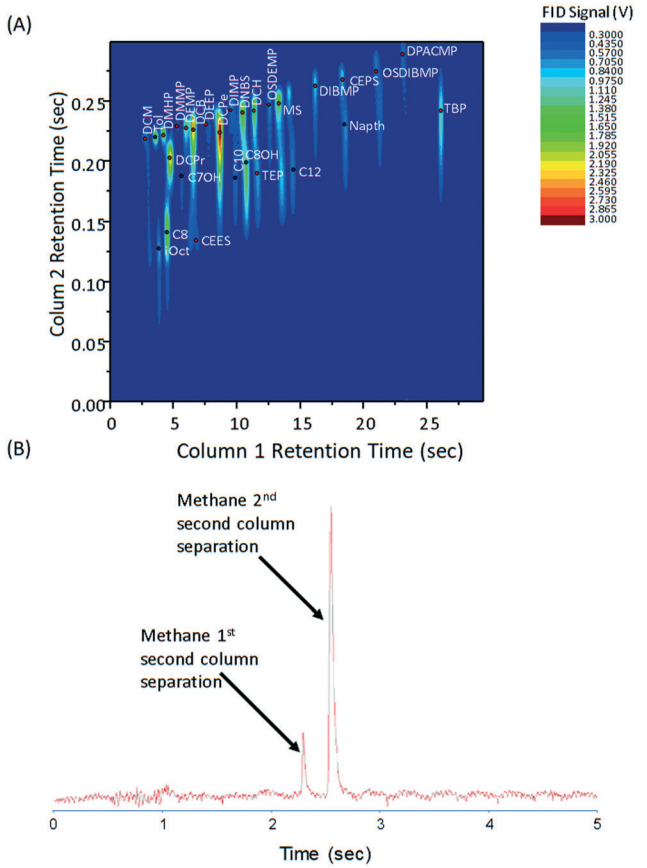

Fig. 2 (A) Initial demonstration of the simplified stop-flow manifold utilizing a pair of commercial 100 μm i.d. capillary columns to separate 28 components in under 30 seconds. (B) Modulation of methane using microfabricated columns and Neptune research valve manifold.

provided both fluidic interconnections and mechanical support for the columns.

The columns were resistively heated using Minco (Minneapolis, MN) 0.5″ × 0.5″ Kapton Thermofoil heaters (PN - HK5572R13.9L12E) for the 3090 columns, and 0.25″ × 0.25″ Kapton Thermofoil heaters (PN - HK5565R10.0L12B) for the 3030 columns. The columns were heated open loop with a "spike and hold" mechanism. Initially a high voltage spike was applied for several seconds to generate a heating ramp of 5–25 °C s^{-1}. This is followed by a lower hold voltage that maintained the achieved temperature. The applied voltages were adjusted until the desired temperature ramp was achieved.

Fig. 1D shows an SEM of a nanoelectromechanical system (NEMS) resonator sensor developed by the Roukes group at the California Institute of Technology. The resonators consist of a 100 nm-thick suspended silicon nitride film topped by 30 nm of gold, fabricated into a cantilever by electron-beam lithography, liftoff, and plasma etching processing steps; fabrication details have been published previously.[42] The NEMS are excited into mechanical motion thermoelastically *via* an alternating electrical current through the gold film,[43] and the motion is detected electrically by monitoring the piezoresistive strain in the film.[44] By using all-electrical control, the sensor can be fully enclosed into microfluidic flow channels without geometrical restrictions imposed by alternative detection methods, *e.g.* external optical detection methods.

The operating principle of the NEMS is based on mass accretion of the analyte onto the resonator as the chromatographic peak flows over its surface, which is then measured as a shift of the NEMS' mechanical resonance frequency. This accretion can be enhanced through the use of a chemically-selective polymer film of approximately 10–20 nm thick on the resonator surface. For these experiments, DKAP,[43,44] a polymer developed by Sandia to preferentially absorb phosphonates, was deposited onto the surface of the NEMS by drop-coating the polymer in solution and air drying. By using a digital phase-locked-loop circuit,[41] the resonance frequency of the NEMS could be tracked in real time, allowing the sensor to track the chromatographic peak sequences as they exited the second GC column.

An array of 6 of these resonators were packaged in a flow through channel as shown in Fig. 1D that allowed integration with the microfabricated GC×GC system. The sensor packaging has previously been proven effective for allowing NEMS sensors to detect chromatographic peaks with great fidelity using high-speed 1-dimensional GC.[44] The NEMS resonators were first evaluated for response time and then used to evaluate the retention time stability of the system. For this test, the GC×GC assembly was connected to the split/splitless inlet of the Agilent 6890 as before, but the column was connected to the NEMS resonator package instead of the FID. The oven was held isothermal at 82 °C as over 20 000 analyses were completed over 40 days of continuous operation.

Column fabrication and coating

An extensive description of the fabrication of the 3090 and 3030 columns can be found elsewhere[14] and will only be briefly discussed here. The columns were prepared by a two mask deep reactive ion etch (DRIE) process. The first mask was used to pattern a rectangular patch of silicon dioxide at the locations of the inlet and outlet edge connections of the GC column. This layer is used to delay the start of etching at these locations. Without these rectangular delay regions in the ports, the ports would etch considerably deeper than the subsequently patterned GC columns given the well-known dependence of Bosch etch rate on feature size ("reactive ion etch lag" or "RIE lag"). The intent was to make the column and port depths identical. The second mask defines a photoresist layer (AZ9260) aligned to the silicon dioxide delay layer pattern. The photoresist mask contains the spiral-in-spiral out column pattern and the rectangular edge connection geometry. 150 mm diameter <100> silicon wafers were patterned with these two masks such that when they were initially placed in the Bosch RIE system, silicon was exposed in the spiral pattern regions, but the relatively larger edge connection ports were protected and delayed in etching by the silicon dioxide patches. The relative etch rates of silicon

dioxide and silicon, and the RIE lag determine the required thickness of the delay layer silicon dioxide to allow the channel depth and edge connections to be approximately the same depth at the completion of the etch process. The thickness of the silicon dioxide determines when it is consumed in the etch and therefore when the silicon in the edge connection region begins etching. Another method used involved dipping the wafers into buffered oxide etchant (6 : 1 BOE) to remove the exposed silicon dioxide after the channel regions had a suitable head start to allow both feature sizes to reach the same depth. After removing the silicon dioxide, the wafers were rinsed and dried and reinserted into the Bosch etcher to complete the process to the required depth. Following Bosch etching, the wafers were cleaned in 3 : 1 piranha solution, 6 : 1 BOE and were then anodically bonded to a Pyrex glass lid and diced.

Columns were coated using modified versions of the static method initially described by Lambertus[4,9] and detailed in Whiting.[14] In brief, the columns were cleaned with isopropanol then checked for leaks, unimpeded flow, and a continuous channel seal. The columns were then statically coated. The 3090 columns were coated using a solution of ~9.7 mg of 25 000 cSt vinyl-terminated PDMS (Gelest, Inc. Morrisville, PA) in 3.94 mL of methylene chloride and 3.94 mL of pentane that resulted in a film calculated to have a film thickness of ~20 nm. The 3030 columns were coated using a solution of 11.5 mg of 35 000 MW PEG (Sigma-Aldrich, St. Louis, MO) in 3.94 mL of methylene chloride and 3.94 mL of pentane that was calculated to result in a film thickness of ~20 nm. 16 μL of a 5% (w/v) azobisisobutyronitrile (AIBN) in methylene chloride solution was added per 1 mL of coating solution for both column

Table 1 List of analytes used in testing, labels, boiling points, CAS no. and mass injected on column for Fig. 3A

Analyte	Label	Boiling point (°C)	CAS no.	Mass for Fig. 3A (g)
Pentane	C5	36	109-66-0	—
Dichloromethane	DCM	39.8	75-09-2	—
Carbon disulfide	CS2	46	75-15-0	4×10^{-6}
Trichloroethylene	TCE	87.2	79-01-6	5×10^{-10}
Chloroethylphenylsulfide	CEPS	90	5535-49-9	4×10^{-10}
3-Methylhexane	3MH	90.7	589-34-4	2×10^{-10}
2-Butanol	2C4OH	94	78-83-1	3×10^{-10}
Dichloropropane	DCPr	96	78-87-5	4×10^{-10}
iso-Octane	iOct	99	540-84-1	—
Toluene	TOL	111	108-88-3	3×10^{-10}
3,3-Dimethyl-2-butanol	33DM2C4OH	120	464-07-3	3×10^{-10}
Octane	C8	126.4	111-65-9	—
Chlorobenzene	CB	131	108-90-7	3×10^{-10}
Pentanitrile	PN	140	110-59-8	2×10^{-10}
Chloroethylethylsulfide	CEES	156	693-07-2	3×10^{-10}
2-Heptanol	C7OH	161	543-49-7	—
Dichlorobutane	DCB	162	110-56-5	—
Dimethyl hydrogen phosphonate[a]	DMHP	170.5	868-85-9	7×10^{-9}
Decane	C10	174	124–18-5	2×10^{-10}
Dimethyl methylphosphonate[a]	DMMP	181	756-79-6	7×10^{-9}
Dichloropentane	DCPe	182	628-76-2	3×10^{-10}
n-Butylsulfide	NBS	188	544-40-1	3×10^{-10}
Diisopropyl methylphosphonate[b]	DIMP	189	1445-75-6	7×10^{-9}
Diethyl methylphosphonate	DEMP	194	683-08-9	—
Octyl alcohol	C8OH	194.5	111-87-5	—
Undecane	C11	196	1120-21-4	2×10^{-10}
Trimethylphosphate	TMP	197	512-56-1	7×10^{-9}
Diethyl ethylphosphonate	DEEP	198	78-38-6	6×10^{-9}
Dichlorohexane	DCH	208	2163-00-0	3×10^{-10}
Nitrobenzene	NB	211	98-95-3	4×10^{-10}
Nonyl alcohol	C9OH	214	143-08-8	3×10^{-10}
Triethylphosphate	TEP	215	78-40-0	—
Dodecane	C12	216	112-40-3	2×10^{-10}
Napthalene	Napth	218	91-20-3	4×10^{-9}
Methyl salicylate[a]	MS	222	8024-54-2	4×10^{-10}
O,*S*-Diethyl methylphosphonate[b]	OSDEMP	223	2511-10-6	7×10^{-9}
Diethyleneglycol monobutylether	DEGMBE	230	112-34-5	6×10^{-9}
Tetradecane	C14	253	629-59-4	2×10^{-10}
Diisobutyl methylphosphonate[b]	DIBMP	254	7242-56-0	—
O,*S*-Diisobutyl methylphosphonate[b]	OSDIBMP	273.2	100860–55-7	—
Tributylphosphate	TBP	289	126-73-8	—
Dipinacolyl methylphosphonate[b]	DPACMP	306.2	7040-58-6	—

[a] – Purchased through Fisher Scientific from Aldrich. [b] – Purchased through Fisher Scientific from Alfa-Aesar.

chemistries. After coating, the AIBN was thermally activated under hydrogen flow at 120 °C for 10 min to initiate crosslinking. The columns were then evaluated for performance using a mixture of *n*-alkanes (octane, decane, and dodecane) in carbon disulfide.

Materials and procedures

Table 1 shows a list of the chemicals used to evaluate the system, abbreviations used, and boiling point. All chemicals were purchased from Fisher Scientific unless otherwise noted. Samples were prepared by diluting 1–2 μL of analyte with 1–1.5 mL of carbon disulfide. Carbon disulfide was chosen because of the limited sensitivity FIDs have for the solvent.

Results and discussion

High-speed GC×GC manifold development

Fig. 2A shows the initial proof of concept demonstration of the simplified stop-flow manifold utilizing a pair of commercial 100 μm i.d. capillary columns. The comprehensive two-dimensional chromatogram shows the separation of 28 known components covering a boiling point range of 39–306 °C and 2–3 additional unidentified "bonus" peaks – likely due to contamination in the solvent – in less than 30 seconds. A single modulation period for a traditional GC×GC system is often 5–10 seconds long, but utilizing the high-speed modulator, this time period was reduced more than an order of magnitude to 300 ms. Second dimension peak widths range from 10–60 ms in width, and first dimension peaks widths are on the order of a second. The chromatogram shows the anticipated structure with polar analytes retained in the second column relative to non-polar analytes. Fig. 2B shows one of the initial tests with the valve modulator shown in Fig. 1B using microfabricated columns. The coupled system was able to modulate an unretained methane (two slices) peak at ambient temperatures. This demonstrates one advantage of the pneumatic modulators relative to existing thermal modulators; because the modulation is independent of retention factor, even extremely volatile organics such as methane and permanent gasses are modulated with the same efficiency.

Fig. 3A shows the separation of a 29-component mixture covering a boiling point range of 46 to 253 °C on a pair of microfabricated columns using the Staiger valve manifold in less than 7 seconds, and just over 4 seconds after the ensemble holdup time. The first column in this set was heated at roughly 40 °C s^{-1} from 30 °C to 230 °C after a 0.5 s hold. The second column was heated from 30 °C to 60 °C at 6 °C s^{-1} after a 1 s hold. The difference in column temperatures achieved is due to several factors including the placement of the thermocouple on each column, the variance in film thickness from column to column due to variation in column roughness, and the custom nature of the coating process. The applied voltages for the spike were incrementally modified to achieve the desired separation and analysis time.

The resulting separation shown in Fig. 3A is significantly faster than the chromatogram demonstrated by the commercial columns in Fig. 2A due to the significantly reduced flow restriction of the high aspect ratio microfabricated columns while maintaining much of the resolving power of high resolution commercial columns. The modulation period was reduced to 160 ms by allowing analytes to "wrap around" from one modulation to the next to maximize utilization of available peak capacity to minimize total analysis time. Peak widths on the second column range from 10–60 ms, and the first column peak widths are all less than 1 second. There is some significant peak broadening for the higher boiling point phosphonates and polar analytes; part of this is due to overloading the column because of poor detector sensitivity especially for the phosphonates. Table 1 lists the calculated mass injected onto the column for all of the components in the mixture.

Fig. 3B shows the separation of a series of alkanes – octane (C8), decane (C10), undecane (C11), dodecane (C12) and tetradecane (C14) – optimized to maximize peak capacity. Peak widths and retention times for the alkanes are given in Table 2. The separation on the first column is best described as a temperature programmed separation as a result Trennzahl numbers (TZ) were used to calculate the number of perfectly spaced peaks with a resolution, R_s, of one that can fit between a pair of *n*-alkane peaks.[45] The peak capacity for the first column is the sum of the TZ. The equation is given by eqn (2) below for a series of alkanes, where t_1 and t_2 are the

$$n_p = \sum \frac{1.18}{R_s}\left(\frac{t_2 - t_1}{w_1 + w_2}\right) \quad (2)$$

retention times for the pair of alkanes and w_1 and w_2 are the full width at half height for each pair of alkanes. The second dimension in most GC×GC separations is approximated as an isothermal separation. As a result, the peak capacity was calculated using eqn (3) below for each alkane

$$n_p = 1 + \frac{\sqrt{N}}{4R_s}\ln\left(\frac{t_r}{t_m}\right) \quad (3)$$

where N is the number of theoretical plates, t_r is the retention time of the alkane, and t_m is the holdup time of the second column. In order to calculate the retention time of the last eluting compound (C14), which was allowed to wrap around to minimize the total analysis time, the retention time was calculated as the actual time plus the modulation period to account for wrap around. The total peak capacity was calculated as the product of the first column peak capacity and the average second column peak capacity. For a resolution of 1.0, the calculated peak capacity was 306–30.6 on the first column and 10.0 on the second column – for a separation of just over 6 seconds.

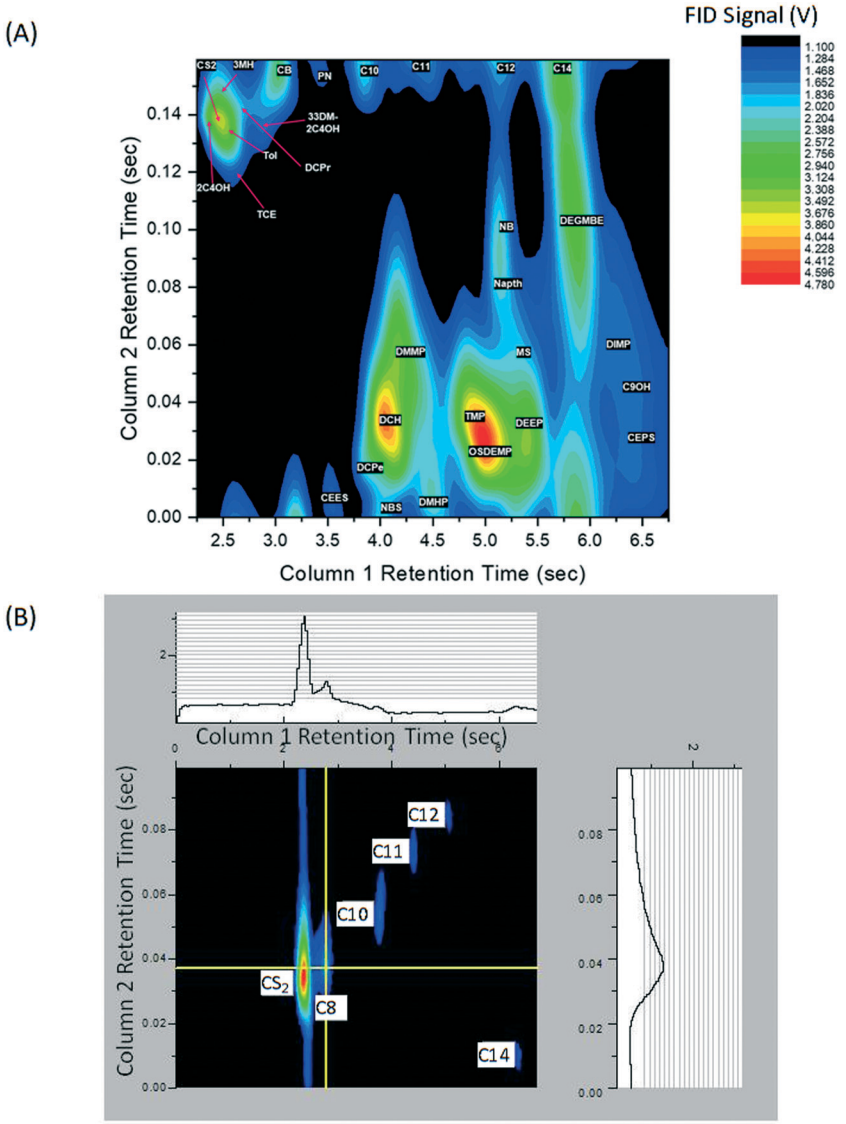

Fig. 3 (A) Two-dimensional separation of 29 components in less than 7 seconds using a pair of microfabricated columns and the Staiger valve manifold. (B) Separation of a series of alkanes optimized for peak capacity resulting in a calculated peak capacity ~300 in just over 6 seconds.

High-speed, microfabricated GC×GC-NEMS resonator integration

The microfabricated GC×GC system was integrated with the Caltech NEMS resonator. Fig. 4A shows the isothermal separation of six components, four known targets and two unknown contaminants detected by the NEMS resonator. There was no apparent additional peak broadening from the use of the NEMS resonators. Fig. 4B shows individual second dimension slices A and B corresponding to the similarly labeled lines in Fig. 4A. The slices show second dimension peaks as narrow as 8 ms wide (slice A) with no discernable peak distortion due to undersampling by the detector.

Table 2 Retention times and peak widths for alkanes for Fig. 3B

Analyte	Retention time – column 1 (s)	Full width half height – column 1 (s)	Retention time – column 2 (s)	Full width half height – column 2 (s)
Octane (C8)	2.77	0.13	0.038	0.014
Decane (C10)	3.79	0.10	0.054	0.012
Undecane (C11)	4.41	0.078	0.073	0.008
Dodecane (C12)	5.07	0.056	0.084	0.006
Tetradecane (C14)	6.35	0.046	0.0104	0.006

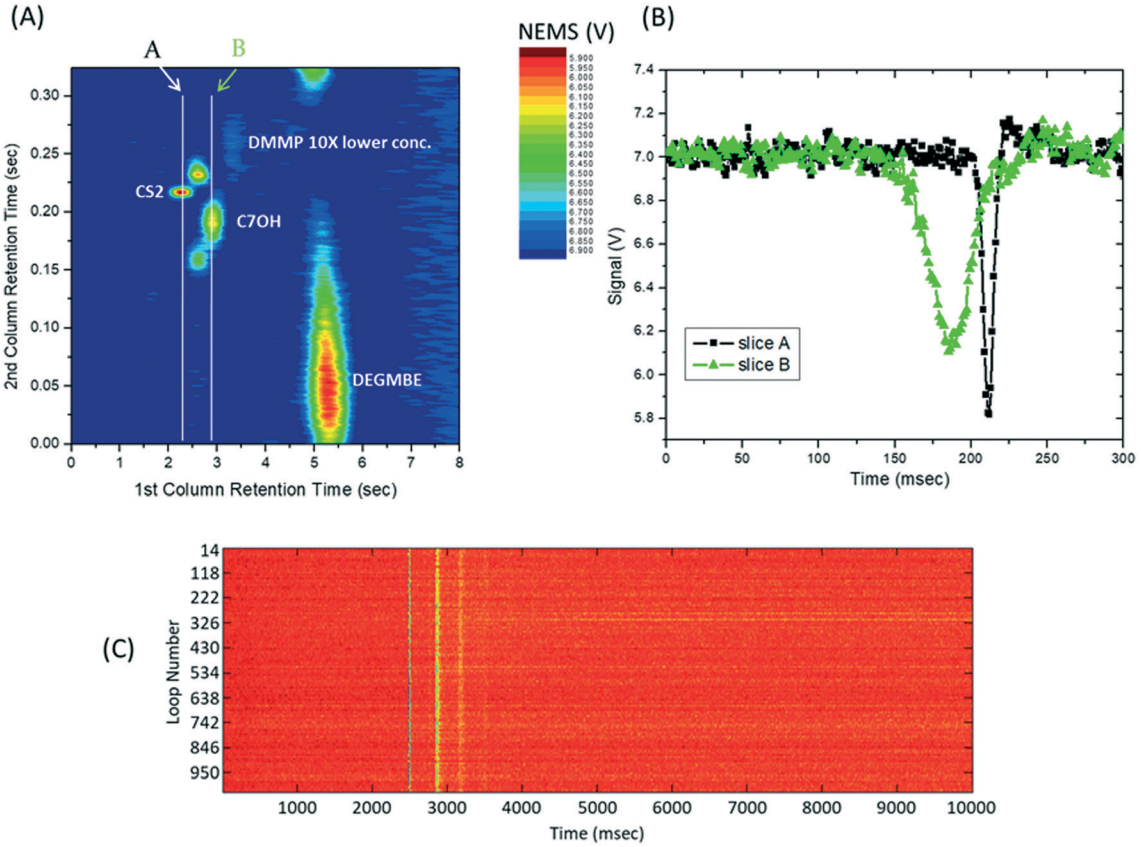

Fig. 4 (A) A 6 second two-dimensional isothermal separation of 6 components utilizing a Caltech NEMS resonator coated with DKAP for detection. (B) Individual slices from 4A showing the second-dimension peak widths including a 8 ms wide peak with no apparent distortion due to under sampling in trace A. (C) Data from one subset (~1000 DMMP only analyses) of a large (>20 000 analyses over 40 days) test for the evaluation for modulator and NEMS stability. The vertical axis is the run number in this subset, *i.e.* loop 14 corresponds to the 14th run of DMMP only. The horizontal axis is the data point in an individual run with data collected at 1 kHz, *i.e.* sample number 10 000 corresponds to the data point for the frequency of the resonator at 10 000 seconds into the run. The amplitude corresponds to the amplitude of the data point in the loop number on the vertical axis and the sample number on the horizontal axis. Therefore, the vertical stripes at ~2600, 2900, 3200, and 3500 correspond to peak apexes for CS2 and DMMP.

Fig. 4C shows data from one subset (~1000 DMMP-only analyses) of a large (>20 000 analyses over 40 days) test for the evaluation for modulator and NEMS stability. The NEMS resonators and columns were run isothermally at 82 °C to minimize variation due to thermal cycling of the microfabricated columns. The vertical axis of the plot shown in Fig. 4C is the run number in this subset, *i.e.* loop 14 corresponds to the 14th run of DMMP only. These loops were dispersed regularly throughout the entire 20 000 set. The horizontal axis of the plot shown in Fig. 4C is the data point in an individual run with data collected at 1 kHz, *i.e.* sample number 10000 corresponds to the data point for the frequency of the resonator at 10 000 seconds into the run. The amplitude of the plot shown in Fig. 4C corresponds to the amplitude of the data point in the loop number on the vertical axis and the sample number on the horizontal axis. Therefore, the vertical stripes at ~2600, 2900, 3200, and 3500 ms correspond to peak apexes for CS2 and DMMP. The perpendicularity of the lines corresponds to the time stability of the microfabricated GC×GC modulator. The signal strength stability is denoted by the uniformity of the color of each stripe and the background. This signal stability corresponds to a convolution of several factors – the stability of the sensor response, the stability of the sample introduction method, and the stability of the sample concentration. Even with these confounding factors the sensor response appears very stable over the course of 40 days of continuous operation.

Conclusions

For portable applications where the power, speed and consumable demand of traditional thermal modulators makes GC×GC a challenge, stop-flow pneumatic modulators offer a low-power, high-speed, alternative. While the demonstration of this technique presented here utilizes hydrogen carrier gas to maximize the high-speed performance potential, the use of scrubbed ambient air could, and has been demonstrated in previous work by Whiting and Sacks[38] to enable consumable-free applications at the trade of analysis time to achieve the same or greater resolution. The trade-off for this size, weight and power (SWAP) advance is a loss of detectability enhancement that are present in flow and thermally modulated systems. The use of

microfabricated columns coupled with very sensitive low-power NEMS resonators enable the development of a powerful analytical tool in a handheld form factor suitable for applications where size, weight, power, and speed are important such as military, environmental, and space applications.

Author contributions

Formal analysis: J. W., E. M., J. R.; methodology: J. W., J. R., R. S.; writing-original draft: J. W., R. S.; writing-review and editing: H. M., K. A.; investigation: J. W., E. M., C. F.; data curation: J. W., E. M., J. R.; conceptualization: J. W., R. S., E. M., M. R.; resources: R. M., M. M., J. A., C. W., A. S., D. P., D. G., D. W.; software: S. H., E. M.

Conflicts of interest

There are no conflicts to declare.

Acknowledgements

This work was supported by the Defense Advanced Research Projects Agency Microsystems Technology Office (DARPA MTO) under Micro Gas Analyzers Program contract number 017040518. Sandia National Laboratories is a multimission laboratory managed and operated by National Technology & Engineering Solutions of Sandia, LLC, a wholly owned subsidiary of Honeywell International Inc., for the U.S. Department of Energy's National Nuclear Security Administration under contract DE-NA0003525. This paper describes objective technical results and analysis. Any subjective views or opinions that might be expressed in the paper do not necessarily represent the views of the U.S. Department of Energy or the United States Government. The authors gratefully acknowledge consultations with Professor Richard Sacks at the University of Michigan, who inspired this avenue of research; and the assistance of Atilla Kiss and Akos Sule at Neptune Research. A part of this paper was supported by Sandia National Laboratories' Laboratory Directed Research and Development (LDRD) project # 199974.

References

1 S. C. Terry, J. H. Jerman and J. B. Angell, *IEEE Trans. Electron Devices*, 1979, **26**, 1880–1886.
2 A. Ghosh, C. R. Vilorio, A. R. Hawkins and M. L. Lee, *Talanta*, 2018, **188**, 463–492.
3 B. P. Regmi and M. Agah, *Anal. Chem.*, 2018, **90**, 13133–13150.
4 S. Reidy, G. Lamertus, J. Reece and R. Sacks, *Anal. Chem.*, 2006, **78**, 2623–2630.
5 A. D. Radadia, R. I. Masel, M. A. Shannon, J. P. Jerrell and K. R. Cadwallader, *Anal. Chem.*, 2008, **80**, 4087–4094.
6 M. Nishino, Y. Takemori, S. Matsuoka, M. Kanai, T. Nishimoto, M. Ueda and K. Komori, *IEEJ Trans. Electr. Electron. Eng.*, 2009, **4**, 358–364.
7 C. J. Lu, W. H. Steinecker, W. C. Tian, M. C. Oborny, J. M. Nichols, M. Agah, J. A. Potkay, H. K. L. Chan, J. Driscoll, R. D. Sacks, K. D. Wise, S. W. Pang and E. T. Zellers, *Lab Chip*, 2005, **5**, 1123–1131.
8 A. D. Radadia, R. D. Morgan, R. I. Masel and M. A. Shannon, *Anal. Chem.*, 2009, **81**, 3471–3477.
9 G. R. Lambertus, R. J. Simonson, A. Bhushan, E. Overton, C. Hasselbrink, R. D. Sacks and J. J. Whiting, *MSS in preparation*, 2019.
10 G. E. Spangler, *Anal. Chem.*, 1998, **70**, 4805–4816.
11 M. J. E. Golay, *J. Chromatogr. A*, 1981, **216**, 1–8.
12 G. E. Spangler, *J. Microcolumn Sep.*, 2001, **13**, 285–292.
13 H. Ahn and S. Brandani, *AIChE J.*, 2005, **51**, 1980–1990.
14 A. Staton, J. Anderson, R. Manginell, C. Washburn, C. Fix, J. Strong, D. Porter, R. J. Simonson and J. J. Whiting, *MSS in preparation*, 2019.
15 S. J. Kim, S. M. Reidy, B. P. Block, K. D. Wise, E. T. Zellers and K. Kurabayashi, *Lab Chip*, 2010, **10**, 1647–1654.
16 S.-J. Kim, G. Serrano, K. D. Wise, K. Kurabayashi and E. T. Zellers, *Anal. Chem.*, 2011, **83**, 5556–5562.
17 G. Serrano, D. Paul, S.-J. Kim, K. Kurabayashi and E. T. Zellers, *Anal. Chem.*, 2012, **84**, 6973–6982.
18 W. R. Collin, A. Bondy, D. Paul, K. Kurabayashi and E. T. Zellers, *Anal. Chem.*, 2015, **87**, 1630–1637.
19 J. J. Whiting, C. S. Fix, J. M. Anderson, A. W. Staton, R. P. Manginell, D. R. Wheeler, E. B. Myers, M. L. Roukes and R. J. Simonson, *Transducers*, 2009, 1666–1669.
20 J. Phillips, D. Luu and J. B. Pawliszyn, *Anal. Chem.*, 1985, **57**, 2779–2787.
21 J. Phillips, R. B. Gaines, J. Blomberg, F. W. M. van der Widen, J. M. Dimandja, V. Green, J. Granger, D. Patterson, L. Racovalis, H. J. de Geus, J. de Boer, P. Haglund, J. Lipsky, V. Sinha and E. B. Ledford, Jr., *J. High Resolut. Chromatogr.*, 1999, **22**, 3–10.
22 P. J. Marriott and R. M. Kinghorn, *Anal. Chem.*, 1997, **69**, 2582–2588.
23 E. B. Ledford, Jr. and C. Billesbach, *J. High Resolut. Chromatogr.*, 2000, **23**, 202–204.
24 C. A. Bruckner, B. J. Prazen and R. E. Synovec, *Anal. Chem.*, 1998, **70**, 2796–2804.
25 J. V. Seeley, F. J. Kramp and K. S. Sharpe, *J. Sep. Sci.*, 2001, **24**, 444–450.
26 J. V. Seeley, N. E. Schimmel and S. K. Seeley, *J. Chromatogr. A*, 2018, **1536**, 6–15.
27 P. McA. Harvey, R. A. Shellie and P. R. Haddad, *J. Chromatogr. Sci.*, 2010, **48**, 245–250.
28 M. Libardoni, J. H. Waite and R. Sacks, *Anal. Chem.*, 2005, **77**, 2786–2794.
29 M. Libardoni, E. Hasselbrink, J. H. Waite and R. Sacks, *J. Sep. Sci.*, 2006, **29**, 1001–1008.
30 C. S. Fix, Comprehensive Multidimensional Gas Chromatography and Modulator Development for Portable Instrumentation, *Ph.D. dissertation*, The University of Michigan, 2009.
31 R. Sacks, C. Coutant, T. Veriotti and A. Grall, *J. High Resolut. Chromatogr.*, 2000, **23**, 225–234.
32 T. Veriotti and R. Sacks, *Anal. Chem.*, 2000, **72**, 3063–3069.
33 C. Coutant and R. Sacks, *Anal. Chem.*, 2000, **72**, 5450–5458.

34 T. Veriotti, M. McGuigan and R. Sacks, *Anal. Chem.*, 2001, **73**, 279–285.
35 J. J. Whiting, C. J. Lu, E. T. Zellers and R. D. Sacks, *Anal. Chem.*, 2001, **73**, 4668–4675.
36 H. Smith and R. Sacks, *J. Sep. Sci.*, 2002, **25**, 37–44.
37 T. Veriotti and R. Sacks, *Anal. Chem.*, 2001, **73**, 3045–3050.
38 J. Whiting and R. Sacks, *Anal. Chem.*, 2002, **74**, 246–252.
39 C. J. Lu, J. Whiting, R. D. Sacks and E. T. Zellers, *Anal. Chem.*, 2003, **75**, 1400–1409.
40 J. Harynuk and T. Gorecki, *J. Sep. Sci.*, 2004, **27**, 431–441.
41 M. Li, H. X. Tang and M. L. Roukes, *Nat. Nanotechnol.*, 2007, **2**, 114–120.
42 I. Bargatin, I. Kozinsky and M. L. Roukes, *Appl. Phys. Lett.*, 2007, **90**, 093116.
43 R. P. Manginell, D. R. Adkins, M. W. Moorman, R. Hadizadeh, D. Copic, D. A. Porter, J. M. Anderson, V. M. Hietala, J. R. Bryan, D. R. Wheeler, K. B. Pfeifer and A. Rumpf, *J. Microelectromech. Syst.*, 2008, **17**, 1396–1407.
44 M. Li, E. B. Myers, H. X. Tang, S. J. Aldridge, H. C. McCaig, J. J. Whiting, R. J. Simonson, N. S. Lewis and M. L. Roukes, *Nano Lett.*, 2010, **10**, 3899–3903.
45 R. Sacks, in *Modern Practice of Gas Chromatography*, ed. R. L. Grob and E. Barry, Wiley, Hoboken, 4th edn, 2004, ch. 5, pp. 229–274.